ChemPubSoc Europe

DOI: 10.1002/chem.201502714

CHEMISTRY A European Journal Full Paper

Semiconductors

Towards Organized Hybrid Nanomaterials at the Air/Water Interface Based on Liquid-Crystal/ZnO Nanocrystals

Jan Paczesny,*[a] Małgorzata Wolska-Pietkiewicz,[b] Ilona Binkiewicz,[a, b] Zbigniew Wróbel,[a] Monika Wadowska,[a] Kinga Matuła,[a] Igor Dzięcielewski,[c] Damian Pociecha,[d] Julita Smalc-Koziorowska,[c] Janusz Lewiński,*[a, b] and Robert Hołyst*[a]

Abstract: The ability to self-assemble nanosized ligand-stabilized metal oxide or semiconductor materials offers an intriguing route to engineer nanomaterials with new tailored properties from the disparate components. We describe a novel one-pot two-step organometallic approach to prepare ZnO nanocrystals (NCs) coated with deprotonated 4-(dodecyloxy)benzoic acid (i.e., an X-type liquid-crystalline ligand) as a model LC system (termed **ZnO-LC1 NCs**). Langmuir and Langmuir–Blodgett films of the resulting hybrids are investigated. The observed behavior of the ZnO NCs at the air/water interface is rationalized by invoking a ZnO-interdigitation process mediated by the anchored liquid-crystalline shell. The ordered superstructures form according to mechanism based on a **Z**nO-**i**nterdigitation **p**rocess mediated by **l**iquid **c**rystals (termed ZIP-LC). The external and directed force applied upon compression at the air/water interface and the packing of the ligands that stabilize the ZnO cores drives the formation of nanorods of ordered internal structure. To study the process in detail, we follow a nontraditional protocol of thin-film investigation. We collect the films from the air/water interface in powder form (**ZnO-LC1 LB**), resuspend the powder in organic solvents and utilize otherwise unavailable experimental techniques. The structural and physical properties of the resulting superlattices were studied by using electron microscopy, atomic force microscopy, X-ray studies, dynamic light scattering, thermogravimetric analysis, UV/Vis absorption, and photoluminescence spectroscopy.

Introduction

Usually self-assembly processes are related to the interactions between different functional molecules/groups. An additional level of tailor ability in the design of hierarchical structures or multidirectional arrangements can be achieved by the implementation of inorganic–organic core-shell colloidal nanocrystals. The ability to self-assemble nanosized ligand-stabilized metal oxide or semiconductor materials offers an intriguing route to engineer nanomaterials with new tailored properties from the disparate components. In this regard, the Langmuir and Langmuir–Blodgett techniques, which combine both of the essential bottom-up assembly approaches, namely, self-assembly and directed-assembly, could be regarded as ideal methods for the preparation of well-ordered nanomaterials characterized by the required structure and desired remarkable properties.[1] The utility of these techniques for the manipulation of semiconductor nanocrystals was first reported by Bawendi and co-workers.[2,3] The authors reported the formation of densely packed monolayer arrays of CdSe nanocrystallites[2] and the subsequent self-organization into three-dimensional colloidal crystals.[3] A similar approach at the liquid interfaces was used also for the ordering of other semiconductor nanocrystallites into superlattices; however, the resulting structures were mostly photoinactive.[4]

Nanocomposites that consist of inorganic nanocrystals (NCs) and liquid crystals (LCs) have been studied for their applications in devices for photovoltaic and display technologies. The advantages of these two classes of material can be effectively combined, or even their properties enhanced, relative to the individual components and can also provide new functional nanostructures.[5] The self-organizing properties of the liquid-crystalline coating[6] is also the driving force that leads to the self-assembly of the nanoparticles into hierarchical structures.[5] Zinc oxide (ZnO) due to its unique physicochemical properties and biocompatibility is one of the most promising semiconductor materials for nanostructure preparation.[7] The inherent

[a] *Dr. J. Paczesny, I. Binkiewicz, Z. Wróbel, M. Wadowska, K. Matuła, Prof. J. Lewiński, Prof. R. Hołyst*
Institute of Physical Chemistry, Polish Academy of Sciences
Kasprzaka 44/52, 01-224 Warsaw (Poland)
E-mail: jpaczesny@ichf.edu.pl
rholyst@ichf.edu.pl

[b] *M. Wolska-Pietkiewicz, I. Binkiewicz, Prof. J. Lewiński*
Faculty of Chemistry, Warsaw University of Technology
Noakowskiego 3, 00-664, Warsaw (Poland)
E-mail: lewin@ch.pw.edu.pl

[c] *I. Dzięcielewski, Dr. J. Smalc-Koziorowska*
Institute of High Pressure Physics, UNIPRESS
Polish Academy of Sciences, Sokołowska 29/37
01-142 Warsaw (Poland)

[d] *Dr. D. Pociecha*
Faculty of Chemistry, University of Warsaw
Pasteura 1, 02-093 Warsaw (Poland)

Supporting information for this article is available on the WWW under http://dx.doi.org/10.1002/chem.201502714.

physicochemical properties of ZnO NCs are dependent on a variety of factors, including chemical composition, crystallinity, size-distribution, shape, and surface capping by the organic ligand. All these factors can be highly affected by the synthetic procedure used; therefore, over the last decade much attention has been paid to the development of methods for the preparation of ZnO NCs.[7,8] In this regard, the preparation, processability, characterization, and application of ZnO NCs combined with liquid-crystalline molecules is an emerging field. For example, ZnO nanorod/LC nanocomposites for photovoltaic applications have been prepared by marrying ZnO nanoparticles with a liquid-crystalline host in the desired percentage by weight.[9] Only very recently, Kahn and co-workers reported the first successful hybridization of liquid-crystalline molecules with small-sized ZnO NCs[10] and the use of a LC system as a templating agent for the preparation of ZnO NCs.[11] Notably, the passivating LC systems in all the above-mentioned cases act as a L-type neutral ligand.[12] To the best of our knowledge, there is only one example of an effective modification of ZnO NC surfaces by a X-type liquid-crystalline ligand, which was obtained by using a ligand-exchange reaction and grafting mesogenic units around the ZnO NC cores.[13] Only very recently, we developed a general one-pot self-supporting organometallic strategy to prepare ZnO NCs coated with a vast array of monoanionic organic ligands.[14] We wondered whether this approach would be applicable to the preparation of LC–ZnO NC hybrids, and we report herein on photoactive ZnO NCs coated with an X-type liquid-crystalline ligand as a model LC system. Langmuir and Langmuir-Blodgett films of the resulting model LC system at the air/water interface and on solid substrates were also investigated. Consequently, we aim to prove that control over compression parameters and careful selection of capping ligands can introduce order into processes that occur at the air/water interface. To the best of our knowledge, the only work on the formation of ZnO superstructures at the air/water interface reported the formation of photoinactive ZnO nanorods, which was driven by the non-symmetrical shape of the utilized nanoparticles.[15]

Results and Discussion

The ZnO NCs coated with an X-type liquid-crystalline ligand were obtained in one-pot two-step synthetic procedure (see Figure 1 and see the Supporting Information for the experimental details). The first step involved the synthesis of a RZnX complex in an equimolar reaction between commercially available Et_2Zn and 4-(dodecyloxy)benzoic acid (**LC1-H**) in THF. The solution of the RZnX precursor was exposed to air to initiate transformations that led to ZnO NCs coated with monoanionic **LC1** moieties (**ZnO-LC1 NCs**). The structural and physical properties of **ZnO-LC1 NCs** were studied by using electron microscopy (SEM, TEM), atomic force microscopy (AFM), X-ray studies (small-angle X-ray scattering (SAXS), powder X-ray diffraction (PXRD)), dynamic light scattering (DLS), thermogravimetric analysis (TGA), UV/Vis absorption, and photoluminescence (PL) spectroscopy.

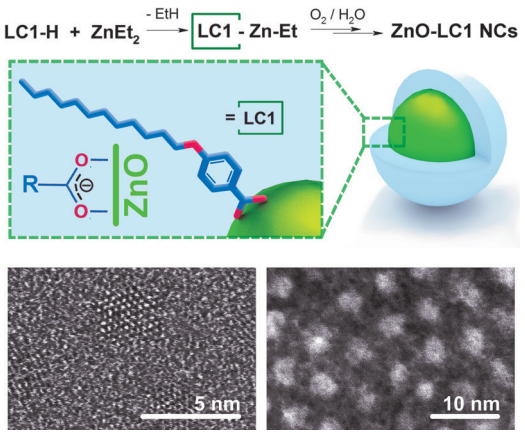

Figure 1. One-pot two-step synthetic procedure for the fabrication of LC1-coated NCs denoted as **ZnO-LC1 NCs**. HRTEM micrographs of the as-prepared **ZnO-LC1 NCs**.

The high-resolution TEM (HRTEM) micrographs of **ZnO-LC1 NCs** show well-dispersed and spherically shaped nanoparticles with a core mean diameter of 3.3 ± 0.2 nm (Figure 1). The crystalline, Wurtzite-type nature of these material is substantiated by the existence of crystal planes in the particles. The SAXS patterns recorded under dilute conditions gave a core diameter of 2.7 ± 0.5 nm (see Figure S3 in the Supporting Information). The hydrodynamic diameter of the ZnO core capped with **LC1** was 6.2 ± 2 nm for the particles dispersed in THF (Figure 2a). PL and UV/Vis spectra of **ZnO-LC1 NCs** are shown in

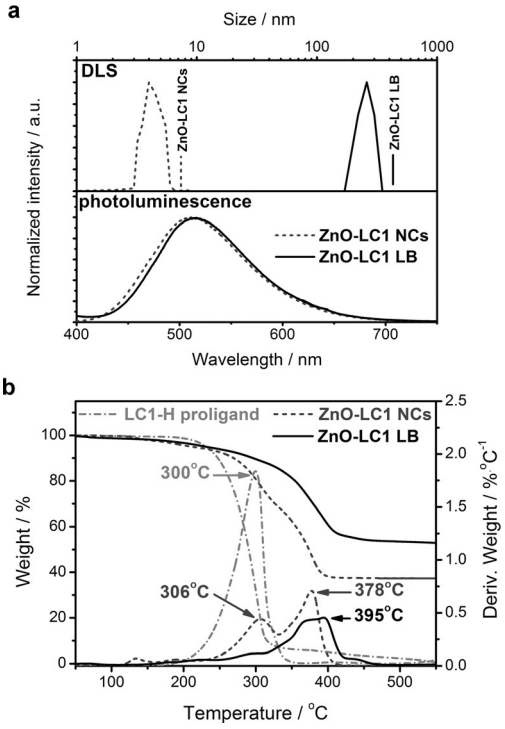

Figure 2. a) Results of DLS measurements together with PL spectra of **ZnO-LC1 NCs**, and **ZnO-LC1 LB** and b) TGA of **LC1-H**, **ZnO-LC1 NCs**, and **ZnO-LC1 LB**.

Figure 2a and Figure S10 (see the Supporting Information), respectively. The ZnO nanocrystals revealed a broad absorption that dropped at $\lambda = 316$ nm in the UV region and PL spectrum emission peaks centered at $\lambda = 512$ nm. In the TGA profile of **ZnO-LC1 NCs**, one main decomposition step with two overlapping components at 306 and 378 °C was observed (Figure 2b). The decomposition process was completed with a total weight loss of 37.3% The TGA and optical data are also discussed in the context of differences between the initial **ZnO-LC1 NCs** and ZnO Langmuir–Blodgett thin films (see below).

The Langmuir–Blodgett technique was used for further study of the thin films based on the well-characterized **ZnO-LC1 NCs** at the air/water interface and on solid substrates. In a control experiment, pure **LC1-H** proligand molecules did not form stable films at the air/water interface, and these molecules tended to drown into the water subphase (see the Supporting Information). This outcome confirms that any recorded surface pressure—molecular area (π–A) isotherms represented the compression of **ZnO-LC1 NCs**. Directly after the application of a suspension of NCs in THF onto the air/water interface, large structures were visible by means of Brewster angle microscopy (BAM). The aggregates spread within 30 minutes (see Figure S5 in the Supporting Information) and then the films were compressed. The π–A isotherms were recorded for different amounts of **ZnO-LC1 NCs** spread at the interface. The relationship between the contact cross-sectional area (CCSA) and the spreading volume was approximately linear (see the insert of Figure S4 in the Supporting Information). The CCSA values were determined by drawing a tangent to the step section and before the bend of the π–A isotherm. The constant-spreading ability of nanoparticles in this range of spread amounts proved that the studied NCs formed a uniform film when applied to the air/water interface.[16] The shape of the isotherms changed with the change of the amount of the studied NCs applied onto the interface, which was caused by different compression speeds exhibited by a single NC expressed in nm^2 per nanocrystal per second. Similar behavior was previously noticed in case of ZnO nanoparticles caped with dodecanethiol.[17] The kinetic effect was also observed in a number of classical amphiphiles.[18] The complex study on the influence of the experimental parameters (e.g., compression speed and amount of material applied onto the interface) on the compression isotherm was performed by Kwok et al.[19]

At the beginning of the experiment, the area available for each NC was much larger than area occupied by a single NC. The films were transparent and became turbid and visible with the naked eye at around 40 $mN\,m^{-1}$. It appeared impossible to perforate such films because of their great elasticity. To investigate such behavior closely, we transferred films of **ZnO-LC1 NCs** onto silicon wafers at different surface pressures according to the Langmuir–Blodgett method and monitored their morphology by means of SEM analysis. The observations revealed the appearance of aggregates, which were present even at very low values of the surface pressure. The surface concentration and the size of such structures increased upon compression. The structures started to coalesce above around 40 $mN\,m^{-1}$, and the thicknesses of the aggregates varied between 50 and 100 nm (Figure 3d), that is, much more than the

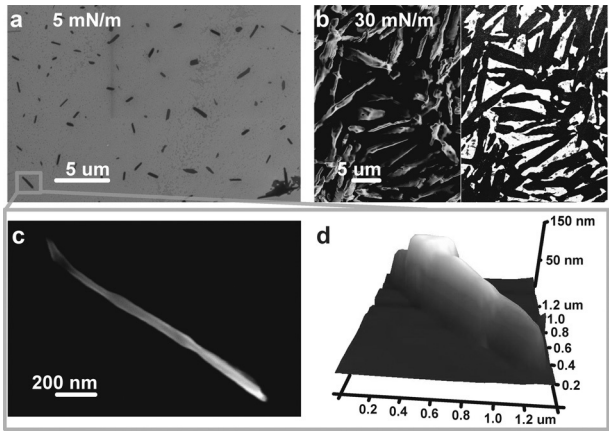

Figure 3. SEM pictures of Langmuir–Blodgett films of **ZnO-LC1 NCs** transferred at a) 5 and b) 30 $mN\,m^{-1}$; c) SEM picture and d) AFM image of the single rodlike aggregate formed at the air/water interface.

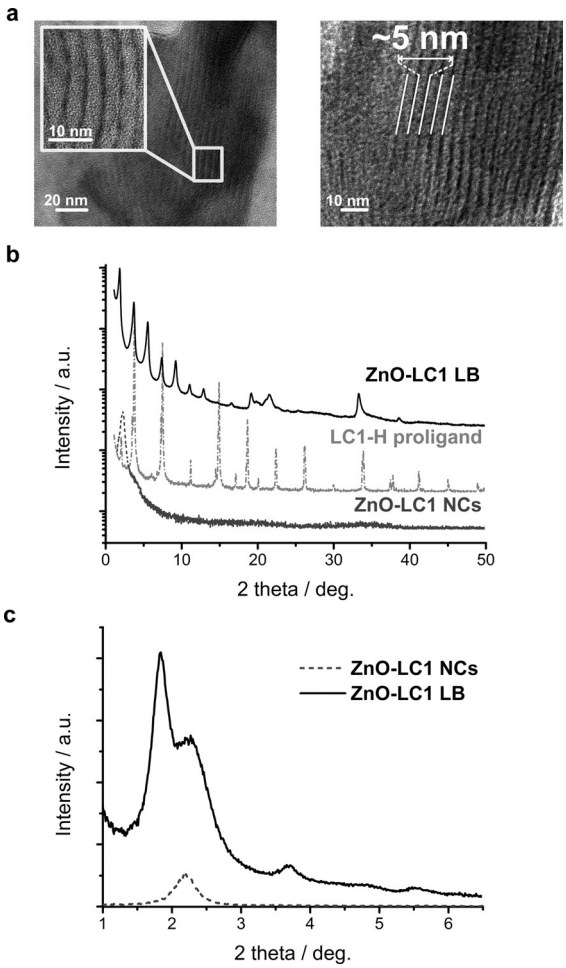

Figure 4. a) HRTEM images that demonstrate the effect of compression of **ZnO-LC1 NCs** at the air/water interface, thus inducing order within the formed **ZnO-LC1 LB** aggregates. b) PXRD and c) SAXS patterns obtained for **ZnO-LC1 NCs** and **ZnO-LC1 LB**. PXRD pattern of LC1-H is shown for comparison.

diameter of a single NC. The morphology of the films transferred at high surface pressure resembled that of ZnO films successfully applied to high-performance field-effect transistors.[20]

Additional experiments were performed to gain insight into the aggregation of ZnO NCs that occur at the air/water interface. The films of **ZnO-LC1 NCs** became turbid and elastic above 40 mN m^{-1}. It was possible to collect the material from the air/water interface as a white powder (denoted as **ZnO-LC1 LB**). This material was suspended in THF and formed stable colloidal suspensions, which were investigated by using DLS, SAXS, PXRD, UV/Vis, PL, and TEM. These analyses allowed us to employ a conventional approach for the characterization of colloidal nanocrystals for the thin-film investigations. The DLS data indicated an aggregation of **ZnO-LC1 NCs** that occur at the air/water interface upon compression and the presence of sub-micrometer structures within **ZnO-LC1 LB**. The recorded sizes of the aggregates approached a limiting value upon sonication and were around two orders of magnitude larger (around 300 nm for **ZnO-LC1 LB**) relative to the diameter of the initial NCs (Figure 2a).

Strikingly, the material collected from the air/water interface retained the photoactivity of the initial **ZnO-LC1 NCs**. The spectroscopic measurements showed almost no changes in the photoluminescence of the **ZnO-LC1 LB** material relative to the initial **ZnO-LC1 NCs**; that is, only a slight shift of the emission maximum was observed (Figure 2a). No change in the optical parameters is usually a strong indication that NCs remained as separate individuals that did not change size during the process. Usually the aggregation of semiconductor NCs results in the formation of photoinactive structures due to the abolition of quantum confinement within particles larger than over a dozen nanometers. In contrast to the previously reported data,[10,11] we faced an apparent paradox, that is, the photoactivity was preserved despite the formation of aggregates. Two possible explanations were considered: 1) the NCs were squeezed/interdigitate together during compression to form aggregates, but without coalescence of the cores; 2) water molecules hydrolyzed the bonds between the ZnO cores and ligand molecules. Without the organic shell, the ZnO cores coalesced due to high surface energy. The observed turbidity of the film appeared upon the formation of macroscopic ZnO, which was not photoactive and did not influence the emission spectra. Because the process was restricted by the geometry of the system not all the NCs aggregated. Some of the NCs became embedded into the nonquantum ZnO matrix.

The TGA profiles for **LC1-H**, **ZnO-LC1 NCs**, and **ZnO-LC1 LB** are shown in Figure 2b. The pure liquid-crystalline proligand decomposes smoothly in one step at around 300 °C. The TGA profile of **ZnO-LC1 NCs** is significantly more complex and exhibits a two-step decomposition pathway. The maxima at around 306 and 378 °C correspond to the protonated and bonded monoanionic forms of the ligand molecules present within the sample, respectively. The thermal-decomposition profile of **ZnO-LC1 LB** has one major decomposition step with a maximum at 395 °C, which corresponds to the bonded ligand. The appearance of only a single decomposition step can be explained in terms of dissolution of the free **LC1-H** molecules in the subphase during transformation from **ZnO-LC1 NCs** to **ZnO-LC1 LB** upon compression at the air/water interface. We note that the pure proligand did not form stable Langmuir films (see the Supporting Information). The TGA data of **ZnO-LC1 LB** shows a total weight loss of 43%. When only the second decomposition step of **ZnO-LC1 NCs** was considered (bonded ligand), the corresponding value was around 40%. The difference in percentage between the weight loss of **ZnO-LC1 NCs** and **ZnO-LC1 LB**, which corresponds to the decomposition of the bonded monoanionic **LC1** ligands, was much too small to explain the core–core aggregation and the formation of macroscopic ZnO. Simple calculations showed that formation of aggregates that were only ten times larger in size relative to the initial NCs should result in a decrease of the mass of the bonded ligand to below 10%; however, the experimental results proved otherwise. This outcome provides comprehensive proof for aggregation mediated by the bonded capping ligands and against core–core aggregation.

On the basis of our previous experience and reported data, we decided to investigate whether the monoanionic liquid-crystalline ligand introduces additional ordering into the whole system. TEM observations of **LC1 ZnO LB** revealed superlattices of ZnO nanocrystals (Figure 4a). The PXRD, SAXS, and X-ray reflectivity (XRR) measurements confirmed that the observed superstructures were not just artefacts. Very intense peaks that are characteristic for lamellar structures were observed for **ZnO-LC1 LB** in the PXRD patterns. On the basis of comparison analysis, we excluded that the peaks originated from pure **LC1-H** or **ZnO-LC1 NCs** (Figure 4b). The SAXS data (Figure 4c) were measured under concentrated conditions for **ZnO-LC1 LB** and **ZnO-LC1 NCs**. The observed peak at around 2.2° corresponds to the average size of the NC (i.e., 40.3 Å), which is in line with the other measurements (see the Supporting Information). Surprisingly, this distance between neighboring NCs was shorter than the sum of the diameter of the core (calculated to be 2.7 nm by means of SAXS under dilute conditions) and two lengths of the **LC1** ligand (ca. 2×2.0 nm). This finding was due to interlinking of the **LC1** ligands from neighboring NCs. In the case of **ZnO-LC1 LB**, additional peaks (ca. 1.85, 3.7, and 5.5°) appeared, thus proving that the ordering of the periodicity of the characteristic length of around 4.8 nm was created upon compression. The recorded XRR patterns were rather unusual and resembled the SAXS patterns (see Figure S6 in the Supporting Information). The characteristic spacing of around 5 nm was also observed in the TEM images. We considered whether the observed SAXS, PXRD, and XRR patterns could originate from the **LC1-H** molecules present in **ZnO-LC1 LB**. The recorded characteristic lengths between the layers did not match the pure **LC1-H** ligand (4.3 and 3.15 nm in the crystalline state and smectic C phase, respectively; see the Supporting Information). Moreover, the TGA analysis confirmed that the pure form of the **LC1-H** proligand molecules was not present within **ZnO-LC1 LB**. This finding assured us that the observed lamellar phase within **ZnO-LC1 LB** was formed due to interactions between the ligands at the surface of the ZnO cores.

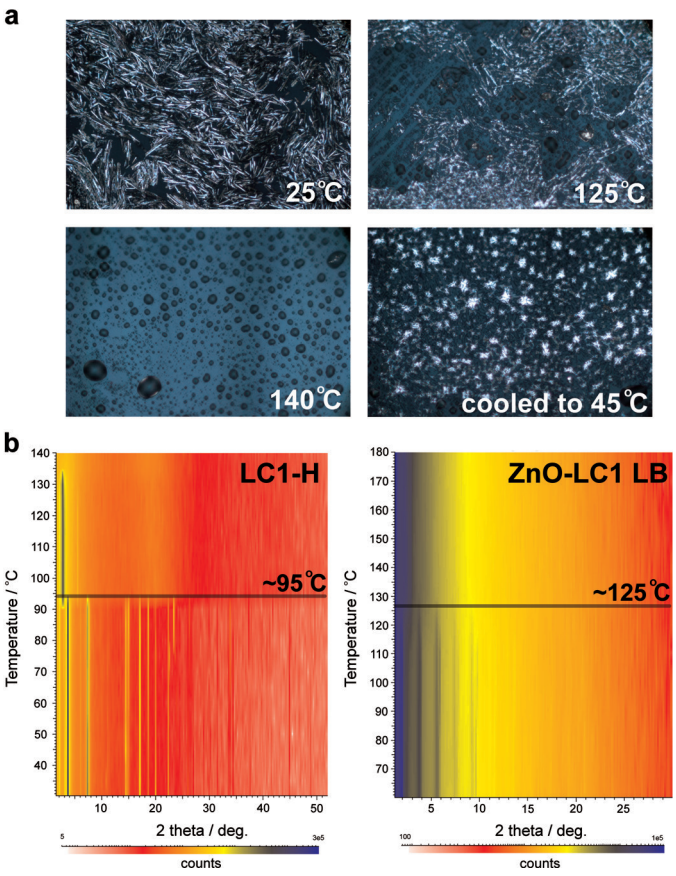

Figure 5. a) Polarized-light microscopy images recorded upon heating from around 25 °C to around 140 °C and cooling to around 45 °C. b) PXRD patterns of **LC1-H** and **ZnO-LC1 LB** taken upon heating. The disappearance of the lamellar phase occurs at around 95 and 125 °C, respectively.

The **ZnO-LC1 LB** film appeared to be birefringent (Figure 5 a). We excluded possibility of unbound **LC1-H** molecules that obscured the observed behavior of **ZnO-LC1 LB**; thus, it appeared that the birefringence was an attribute of the studied superstructures due to interactions of the liquid-crystalline ligands that stabilize the NC ZnO cores.

Observations under polarized light microscope revealed that the rodlike aggregates (i.e., **ZnO-LC1 LB**) started to melt at around 125 °C and formed an isotropic phase in the shape of droplets. This transition was also confirmed by means of PXRD observations. The temperature at which the lamellar phase disappeared was around 125 and 95 °C for **ZnO-LC1 LB** and the **LC1-H** proligand, respectively (Figure 5 b).

Preheated and cooled down below the temperature of the phase transition (125 °C), the **ZnO-LC1 LB** aggregates did not recover the original shape. Rodlike aggregates were also not formed in the experiments, in which the surface pressure was increased by the addition of small volumes of a suspension of the **ZnO-LC1 NCs** (see the Supporting Information) rather than by movement of the barriers of the Langmuir trough. This behavior proved that the observed structures did not appear spontaneously, but that the formation of the **ZnO-LC1 LB** superstructures was driven by compression at the air/water interface.

Two components that might influence the formation of the aggregates at the air/water interface are 1) the tendency of stabilizing ligands for self-assembly and 2) various activities of different crystallographic facets of ZnO cores due to the shape anisotropy. None or very little merging of the ZnO cores was observed, which is in line with observations of the liquid-crystalline-ligand-induced formation of nanorods with ordered internal structures, that is, superlattices. Based on our observations, we proposed a **Z**nO-**i**nterdigitation **p**rocess mediated by **l**iquid **c**rystals (termed ZIP-LC) as a packing mode for the self-assembly mechanism. According to the ZIP-LC mechanism, the formation of ordered ZnO superstructures is driven by the external and directed forces and as a result of packing of the alkyl-tail group of the monoanionic LC molecules attached to the ZnO core. The compression process acts as a zipper that arranges the **ZnO-LC1 NCs** into an ordered pattern. One of the unprecedented feature of this approach is that the self-assembly was conditioned by the properties of the liquid-crystalline ligand; therefore, the ligand-driven mechanism of the coalescence of **ZnO-LC1 NCs** upon compression at the air/water interface was deduced.

Conclusion

We have developed an efficient one-pot two-step organometallic approach toward the synthesis of ZnO NCs coated with a monoanionic liquid-crystalline organic ligand. This study also contributes to understanding of the self-assembly process, that is, we have proven interdigitation of capping ligands over coalescence of cores for hybrid LC/ZnO NCs upon compression at the air/water interface. The study has also demonstrated that the monoanionic form of **LC1-H** on the surface of ZnO NCs maintains the ability to spontaneously form ordered structures, thus distinguishing the LCs. The **ZnO-LC1 NCs** form aggregates upon compression while preserving their photoactivity. Finally, we have proposed a self-assembly mechanism of a **Z**nO-**i**nterdigitation **p**rocess mediated by **l**iquid **c**rystals (ZIP-LC) as a packing mode for the tail group of the stabilizing ligand molecules present on the ZnO NCs surface. Consequently, we believed that the utility of liquid-crystalline properties of the stabilizing ligands for the formation of superlattices of NCs could open up new possibilities for the design and efficient preparation of novel functional nanomaterials. Further studies on self-assembly of hybrid nanomaterials based on LC/ZnO nanocrystals at the air/water interface are in progress.

Experimental Section

General

All the synthetic procedures were carried out in a dry oxygen-free nitrogen atmosphere by using standard Schlenk techniques. All the reagents were purchased from commercial vendors: 4-(dodecyloxy)benzoic acid from Sigma-Aldrich and Et_2Zn from ABCR. THF was stringently dried and distilled prior to use.

Synthesis of ZnO nanocrystals coated with carboxylate ligand (ZnO-LC1 NCs)

ZnO-LC1 NCs were prepared by using the recently developed method in which organozinc precursors of the type of RZnX (X = monoanionic organic ligand) are synthesized in situ and is based on the controlled reactions of this compound with air.[14] Et_2Zn (1 mmol) was added to a stirred solution of 4-(dodecyloxy)benzoic acid (**LC1-H**; 1 mmol) in THF (10 mL) at −78 °C. The reaction mixture was warmed to room temperature and stirred vigorously for further 3 h. The preparation of **ZnO-LC1 NCs** was realized through the exposure of a solution of the obtained organozinc precursor in THF to air at room temperature. Stable **ZnO-LC1 NCs** were obtained within 3 days as a suspension in THF. The estimated size of the NCs stabilized with 4-(dodecyloxy)benzoic acid obtained from various experimental measurements are given in Table S1 (see the Supporting Information).

Langmuir–Blodgett experiments

The Langmuir–Blodgett experiments were performed with the use of a Langmuir trough (5×75 cm; NIMA), equipped with surface-pressure and surface-potential sensors (Trek Inc.), a dipper, and a temperature-control unit. A MiniBAM Brewster angle microscope (BAM; NFT) was used. The system was enclosed in acrylic cabinet to avoid contamination and influence from the external environment. Millipore-filtered water (18.2 MΩ cm at 25 °C) was used as a subphase. To ensure reproducibility of the collected results, the trough was carefully cleaned with $CHCl_3$ and ethanol and then rinsed with water prior to every experiment. Any remaining impurities that were floating on the subphase were removed in a repeated process of putting the barriers as close together as possible and removing the surface layer of water between the barriers with an underpressure aspirator. Rather than a traditional Wilhelmy plate, single-use filter paper stripes were utilized as the surface-pressure sensor. The system was calibrated before each experiment.

ZnO-LC1 NCs suspension and LC1-H solution were applied onto the subphase with a Hamilton microsyringe. The time interval before starting the experiment was 30 min. Afterwards, the films were compressed at a constant rate of 10 $cm^2 min^{-1}$. BAM images were procured in situ. A suspension of the NCs (40 μL) was used in all the experiments for the preparation of films for SEM and AFM imaging. The films were transferred onto silicon wafers (cut along the crystallographic plane <510>) for the SEM and X-ray reflectivity (XRR) measurements. Film deposition was performed according to the Langmuir–Blodgett technique at a dip speed of 5 mm min^{-1} during an upstroke. The polished silicon wafers of very low roughness were cut into 2.5×0.8 cm substrates (purchased from the Institute of Electronic Materials Technology, Warsaw, Poland). Cleaning of the silicon substrate was performed according to the following protocol: The surface was first cleaned with acetone, and then wafers were immersed for at least 30 min in approximately 30% nitric acid. The wafer was rinsed with water and submerged vertically in the trough prior to applying the investigated suspension onto the water surface. Such prepared silicon wafers were hydrophilic.

Characterization by microscopy

SEM images were recorded with use of a Zeiss ULTRA scanning electron microscope in the InLens and low-loss BSE detection modes. AFM analysis was carried out with a multimode scanning probe microscope (Bruker) in the ScanAsyst mode. TEM observations were performed by using conventional high-resolution (HR) TEM and scanning (STEM) techniques on a FEI TECNAI G2 F20 S-TWIN microscope. Cu mesh grids supplied by Quantifoil and a Zeiss Imager A2m polarizing microscope were used.

X-ray diffraction

Powder X-ray diffraction (PXRD) and XRR measurements were performed on a Bruker D8 Discover diffractometer at a wavelength of 1.54 Å. The monochromatic parallel beam was formed by a parabolic Goebel mirror. A scintillation counter and an automatic absorber of the primary beam allowed for a linear dynamic range greater than 10^8 cps. A VANTEC 2000 detector was used to obtain wide-angle diffractograms.

SAXS analysis

Bruker Nanostar system was used for SAXS experiments. The system was equipped with a parallel point beam of CuKα radiation formed by cross-coupled Goebel mirrors and a 3-pinhole collimator, an area detector, VANTEC 2000, and a thermostated sample holder.

Optical measurements

Fluorescence was measured on a Hitachi F-7000 spectrometer. A Hitachi 650–0161 solid-sample holder was used for solid samples. Hitachi U-2910 was used for absorbance measurements.

Thermogravimetric studies

Thermal-stability experiments were performed in an air atmosphere by using open alumina crucibles on a TA Instruments Q600 analyzer.

Acknowledgements

The work was financed by the Ministry of Science and Higher Education of Republic of Poland from the budgetary resources for years 2013–2015 within project Iuventus Plus 3 IP2012 046572. R.H. acknowledges the support from the National Science Centre within Grant Opus 4 (UMO-2012/07/B/ST4/01400). M.W.-P. and J.L. acknowledge the Foundation for Polish Science Team Program cofinanced by the EU "European Regional Development Fund" TEAM/2011-7/8. J.P. was a scholar within the START programme (79.2015) operated by Foundation for Polish Science. Access to AFM was funded by the Foundation for Polish Science under the FOCUS Programme/Grants 3/2010/ Grants.

Keywords: Langmuir–Blodgett films · nanomaterials · liquid crystals · superlattices · surfaces and interfaces · thin films · ZnO nanocrystals

[1] S. Acharya, J. P. Hill, K. Ariga, *Adv. Mater.* **2009**, *21*, 2959–2981.
[2] B. O. Dabbousi, C. B. Murray, M. F. Rubner, M. G. Bawendi, *Chem. Mater.* **1994**, *6*, 216–219.
[3] C. B. Murray, C. R. Kagan, M. G. Bawendi, *Science* **1995**, *270*, 1335–1338.
[4] a) K. M. Gattás–Asfura, C. A. Constantine, M. J. Lynn, D. A. Thimann, X. Ji, R. M. Leblanc, *J. Am. Chem. Soc.* **2005**, *127*, 14640–14646; b) C. Schliehe, B. H. Juarez, M. Pelletier, S. Jander, D. Greshnykh, M. Nagel, A. Meyer, S. Foerster, A. Kornowski, C. Klinke, H. Weller, *Science* **2010**, *329*,

550 – 553; c) N. F. Crawford, R. M. Leblanc, *Coord. Chem. Rev.* **2014**, *263 – 264*, 13 – 24; d) K. Lambert, Y. Justo, J. S. Kamal, Z. Hens, *Angew. Chem. Int. Ed.* **2011**, *50*, 12058 – 12061; *Angew. Chem.* **2011**, *123*, 12264 – 12267.

[5] For reviews, see: a) G. Ungar, C. Tschierske, V. Abetz, R. Hołyst, M. A. Bates, F. Liu, M. Prehm, R. Kieffer, X. Zeng, M. Walker, B. Glettner, A. Żywocinski, *Adv. Funct. Mater.* **2011**, *21*, 1296 – 1323; b) H. K. Bisoyi, S. Kumar, *Chem. Soc. Rev.* **2011**, *40*, 306 – 319; c) S. Saliba, C. Mingotaud, M. L. Kahn, J.-D. Marty, *Nanoscale* **2013**, *5*, 6641 – 6661; d) W. Lewandowski, M. Wójcik, E. Górecka, *ChemPhysChem* **2014**, *15*, 1283 – 1295.

[6] a) W. Pisula, M. Zorn, J. Y. Chang, K. Müllen, R. Zentel, *Macromol. Rapid Commun.* **2009**, *30*, 1179 – 1202; b) C. Tschierske, *Angew. Chem. Int. Ed.* **2013**, *52*, 8828 – 8878; *Angew. Chem.* **2013**, *125*, 8992 – 9047; c) E.-K. Fleischmann, R. Zentel, *Angew. Chem. Int. Ed.* **2013**, *52*, 8810 – 8827; *Angew. Chem.* **2013**, *125*, 8972 – 8991.

[7] a) H. Morkoç, U. Özgür, *Zinc Oxide: Fundamentals, Materials and Device Technology*, Willey-VCH, Weinheim, **2009**; b) A. B. Djurišić, Y. H. Leung, *Small* **2006**, *2*, 944 – 961; c) C. Klingshirn, *ChemPhysChem* **2007**, *8*, 782 – 803; d) B. Ludi, M. Niederberger, *Dalton Trans.* **2013**, *42*, 12554 – 12568.

[8] a) M. L. Kahn, A. Glaria, C. Pages, M. Monge, L. Saint Macary, A. Maisonnat, B. Chaudret, *J. Mater. Chem.* **2009**, *19*, 4044 – 4060; b) B. Weintraub, Z. Zhou, Y. Li, Y. Deng, *Nanoscale* **2010**, *2*, 1573 – 1587; c) A. B. Djurišić, X. Chen, Y. H. Leunga, A. M. C. Ng, *J. Mater. Chem.* **2012**, *22*, 6526 – 6535.

[9] a) K. Yuan, F. Li, L. Chen, Y. Li, Y. Chen, *J. Phys. Chem. C* **2012**, *116*, 6332 – 6339; b) J. Branch, R. Thompson, J. W. Taylor, L. Salamanca-Riba, L. J. Martínez-Miranda, *J. Appl. Phys.* **2014**, *115*, 164313-1-164313 – 5; c) L. J. Martínez-Miranda, J. W. Taylor, L. K. Kurihara, *Mol. Cryst. Liq. Cryst.* **2014**, *594*, 100 – 104.

[10] S. Saliba, Y. Coppel, P. Davidson, C. Mingotaud, B. Chaudret, M. L. Kahn, J.-D. Marty, *J. Mater. Chem.* **2011**, *21*, 6821 – 6823.

[11] a) S. Saliba, P. Davidson, M. Imperor-Clerc, C. Mingotaud, M. L. Kahn, J.-D. Marty, *J. Mater. Chem.* **2011**, *21*, 18191 – 18194; b) S. Saliba, Y. Coppel, M.-F. Achard, C. Mingotaud, J.-D. Marty, M. L. Kahn, *Angew. Chem. Int. Ed.* **2011**, *50*, 12032 – 12035; *Angew. Chem.* **2011**, *123*, 12238 – 12241; c) S. Saliba, Y. Coppel, C. Mingotaud, J.-D. Marty, M. L. Kahn, *Chem. Eur. J.* **2012**, *18*, 8084 – 8091.

[12] J. S. Owen, *Science* **2015**, *347*, 615 – 616.

[13] C. Neaime, M. Prevot, M. Amela-Cortes, V. Circu, F. Grasset, H. Folliot, Y. Molard, *Chem. Eur. J.* **2014**, *20*, 13770 – 13776.

[14] a) M. Wolska-Pietkiewicz, E. Chwojnowska, A. Grala, K. Wójcik, K. Sokołowski, J. Grzonka, Z. Wróbel, A. Rola-Noworyta, I. Justyniak, W. Bury, A. E. H. Wheatley, K. J. Kurzydłowski, J. Lewinski, unpublished results; b) PL Patents 383356 and 383357, **2007**.

[15] M. P. Shortell, H. W. Liu, H. Zhu, E. A. Jaatinen, E. R. Waclawik, *Langmuir* **2010**, *26*, 14472 – 14478.

[16] Z. Hórvölgyi, S. Németh, J. H. Fendler, *Langmuir* **1996**, *12*, 997 – 1004.

[17] L. Naszályi, A. Deák, E. Hild, A. Ayral, A. L. Kovács, Z. Hórvölgyi, *Thin Solid Films* **2006**, *515*, 2587 – 2595.

[18] A. Jyoti, R. M. Prokop, J. Li, D. Vollhardt, D. Y. Kwok, R. Miller, H. Mohwald, A. W. Neumann, *Colloids Surf. A* **1996**, *116*, 173 – 180.

[19] D. Y. Kwok, B. Tadros, H. Deol, D. Vollhardt, R. Miller, M. A. Cabrerizo-Vilchez, A. W. Neumann, *Langmuir* **1996**, *12*, 1851 – 1859.

[20] B. Sun, H. Sirringhaus, *J. Am. Chem. Soc.* **2006**, *128*, 16231 – 16237.

Received: July 13, 2015
Published online on October 2, 2015